Apoptosis (2025) 30:2238–2253
https://doi.org/10.1007/s10495-025-02136-7

DNA damage repair inhibitors boost targeted radionuclide therapy and immunotherapy of prostate cancer

Bin Xu[1] · Lei Tao[1] · Juan Sun[1] · Jiangtao Yang[1] · Fenghua Meng[1] · Zhiyuan Zhong[1,2]

Accepted: 9 June 2025 / Published online: 26 June 2025

Abstract

Targeted radionuclide therapy (TRT) has emerged as a valuable treatment for metastatic castration-resistant prostate cancer (mCRPC) patients. The radioresistance coupled with heterogeneity and immunosuppressive tumor microenvironment of mCRPC, however, greatly restricts the clinical response and anticancer immunity. Here, we found that DNA damage repair inhibitors, in particular ATM inhibitor (ATMi), effectively boost TRT and immunotherapy of prostate cancer. ATMi significantly amplified TRT-induced DNA damage and immunogenic cell death in tumor cells, by impairing double-strand break repair and arresting cell cycle progression, which reshaped the tumor microenvironment and markedly improved tumor inhibition and survival rate in murine RM-1-hPSMA tumor model. Intriguingly, addition of αCTLA-4 antibody further resulted in 71% mice complete regression. TRT in combination with ATMi and αCTLA-4 appeared to boost adaptive and long-lasting anticancer immunity. Our results signify that ATM inhibitor not only sensitizes targeted radionuclide therapy but also effectively augments immune checkpoint inhibitor therapy.

Keywords Prostate cancer · Targeted radionuclide therapy · Radioresistance · DNA damage repair inhibitors · Immune checkpoint inhibitors

Introduction

Prostate cancer (PC) poses considerable threaten to men's health [1, 2]. It is reported that quite a number of prostate cancer patients will experience recurrence and eventually develop into metastatic castration-resistant prostate cancer (mCRPC), for which conventional therapies like chemotherapy and radiotherapy are all ineffective [3–5]. In 2022, targeted radionuclide therapy (TRT), ^{177}Lu-PSMA-617, was approved by the FDA for the treatment of PSMA-positive mCRPC, which started a new era for mCRPC and renewed the interest for TRT [6–10]. A number of new radioligands and strategies have recently been explored to enhance the tumor targeting ability of TRT [11–14]. We have developed a sigma-1 receptor and PSMA dual-targeted radioligand, ^{177}Lu-S1R/PSMA-P, which exhibits superior accumulation and retention in PSMA-positive prostate tumors to single-targeted counterpart [15]. It should be noted, however, that despite its clinical efficacy, TRT induces only partial responses and fail to achieve complete remission in tumor models and in patients [16–18].

While PSMA is highly expressed in many prostate cancer cells and its expression correlates with disease progression, there is substantial variability in PSMA expression among different tumor cells, metastases, and patients [19, 20]. This heterogeneity in PSMA expression has a direct impact on the efficacy of TRT [21–23]. The presence of radioresistance is another challenge for TRT of prostate cancer [24]. DNA damage repair (DDR) mechanisms are key factors underlying radioresistance in tumor cells [24–26]. The radiation dose delivered by TRT decreases over time as the radionuclide decays, and when their DNA repair mechanisms are sufficient to counteract radiation-induced damage,

Bin Xu and Lei Tao have contributed equally to this work.

✉ Fenghua Meng
fhmeng@suda.edu.cn

✉ Zhiyuan Zhong
zyzhong@suda.edu.cn

[1] Biomedical Polymers Laboratory, College of Chemistry, Chemical Engineering and Materials Science, State Key Laboratory of Radiation Medicine and Protection, Soochow University, Suzhou 215123, PR China

[2] College of Pharmaceutical Sciences, Soochow University, Suzhou 215123, PR China

tumor cells will survive. The inhibition of DNA damage repair could enhance the radiation effect to a certain extent [27–30]. The infiltration of immunosuppressive cells in the tumor microenvironment (TME) is another significant contributor to radioresistance, and the suppressive TME also reduces anticancer immune response by TRT [31–33].

In this paper, we report on DNA damage repair inhibitors (DDRi), in particular ATM inhibitor (ATMi), to effectively boost TRT and immunotherapy of malignant murine RM-1-hPSMA prostate cancer model with αCTLA-4 antibody. We systemically studied the effects of two inhibitors, i.e. PARP inhibitor (PARPi) and ATMi, which inhibit single-strand DNA break and double-strand DNA break repair, respectively [34], on sensitizing TRT and altering immunosuppressive TME. We further investigated TRT in combination with DDRi to augment the immune checkpoint inhibitor (ICI) therapy for RM-1-hPSMA tumor. mCRPC exhibited poor response to ICI due to its highly immune-suppressive TME [35, 36]. Interestingly, our results showed that ATMi significantly amplified TRT-induced DNA damage and immunogenic cell death in tumor cells, which reshaped the tumor microenvironment and markedly improved tumor inhibition and survival rate. TRT in combination with ATMi and αCTLA-4 antibody resulted in 71% mice complete regression, which signifies a potent and long-lasting anticancer immunity. TRT-ATMi-ICI combo therapy appears as a potential strategy to cure prostate cancer.

Experimental section

Preparation of ^{177}Lu-S1R-PSMA-P

^{177}Lu-S1R-PSMA-P, was prepared as our previous report with slight modifications [15]. Briefly, 200 µL of 0.4 M sodium ascorbate solution was added to S1R-PSMA-P (0.2 mg/vial), achieving a final concentration of 1 mg/mL. The molar ratio of $^{177}LuCl_3$ to DOTA was adjusted to 1:6 based on the specific activity of $^{177}LuCl_3$. The reaction mixture was placed in a shaking incubator set at 90 °C (400 rpm) and reacted for 10 min.

Effects of combo therapy on the apoptosis, cell cycle, and DNA damage repair

Apoptosis detection: RM-1-hPSMA cells (8×10^4/well) were seeded in 12-well plates and incubated with culture media containing ^{177}Lu-S1R/PSMA-P (5 or 50 µCi/mL), PARPi (2 or 4 µM) or ATMi (10 or 20 nM) for 48 h ($n = 3$, untreated media served as control). After incubation, Annexin V-PE/7-AAD assay kit was added, and apoptosis was determined using a flow cytometer and analyzed with FlowJo V10 software. Positive regions for Annexin V-PE and 7-AAD staining were determined using single-staining positive controls in the kit to distinguish early and late apoptosis.

Cell cycle arrest: RM-1-hPSMA cells (8×10^4/well) were seeded in 12-well plates, and the drug concentrations and incubation protocols were identical to as above. After incubation, cells were stained with propidium iodide (PI) following the manufacturer's instruction. Cell cycle phases were measured using a flow cytometer, and analyzed with ModFit 5.0 software.

DNA damage and repair (γ-H2AX expression): RM-1-hPSMA cells (8×10^4/well) were seeded in 12-well plates, and the drug concentrations and incubation protocols were identical as above. Cells were harvested by trypsinization, fixed, permeabilized, and blocked. Then cells were stained with Anti-Human/Mouse Phospho-H2AX (S139) rabbit monoclonal antibody, washed, and then stained with Alexa Fluor 647-conjugated goat anti-rabbit IgG secondary antibody. Finally, cells were resuspended in PBS for flow cytometry measurements and data analysis using FlowJo V10 software.

RNA-seq analyses of RM-1-hPSMA cells

RM-1-hPSMA cells (8×10^4/well) were seeded in 12-well plates and cultured. Cells were added with media containing ^{177}Lu-S1R/PSMA-P (50 µCi/mL), PARPi (2 µM) or ATMi (10 nM). After incubation for 48 h, cells were washed and lysed in 1 mL TRIzol reagent. Samples were frozen at −80 °C until further processing. RNA-seq library construction, sequencing and alignment were performed by Beijing Novogene. Differentially expressed genes (DEGs), volcano plot generation, Gene ontology (GO) enrichment analyses, and heatmap visualization were conducted using the Novomagic platform. Specifically, DGEs identification was conducted using edgeR (version 3.22.5) with the cutoff criteria set as $|\log_2(\text{Fold Change})| > 1$ and P-value < 0.05. DGEs were visualized through volcano plots. For GO enrichment analyses, DGEs were first functionally categorized, and enrichment was performed using the clusterProfiler package. GO terms significantly enriched compared to the whole-genome background were identified to infer the major biological functions associated with the DGEs. Heatmaps were generated using the pheatmap package in R, where the $\log_2(\text{FPKM} + 1)$ values of DGEs were standardized and subjected to hierarchical clustering for visualization. The raw sequencing data have been deposited in the NCBI SRA under the accession number [PRJNA1247585].

Induction of ICD in RM-1-hPSMA cells by combo therapy

To assess the ICD induction in RM-1-hPSMA cells induced by ^{177}Lu-S1R/PSMA-P (50 µCi/mL) combined with PARPi

(2 μM) or ATMi (10 nM), cells (3×10^4/well) were seeded into 12-well plates and incubated with culture medium containing TRT, PARPi or ATMi ($n = 3$, with untreated medium as the control group). After incubation for 48 h, the culture media were collected for ATP and HMGB1 analyses, and the cells were harvested to assess CRT expression.

The cells were incubated with an α-calreticulin primary antibody for 60 min on ice. After washing, the cells were stained with Alexa Fluor 647-goat anti-rabbit IgG (H + L) secondary antibody, resuspended in PBS, and analyzed by flow cytometry. ATP levels were measured using an enhanced ATP detection kit by measuring chemiluminescence using a microplate reader according to the manual. ATP concentrations of the samples were calculated based on a standard curve. For detecting HMGB1 levels in culture media, Mouse HMGB1 ELISA kit was used according to the manufacturer's instructions. Absorbance was measured at 450 nm (OD450) using a microplate reader, and HMGB1 concentrations were calculated based on a standard curve of solutions with known concentrations.

Impact of released DAMPs of RM-1-hPSMA cells on antigen-presenting cells

To evaluate the impact of DAMPs released after ICD induction in RM-1-hPSMA cells on antigen presentation capacity, BMDCs (1×10^6cells/mL) were seeded onto 12-well plates and incubated overnight. The conditioned media collected from the above experiments were then added to these BMDCs to co-incubate for 6 h. BMDCs were collected by centrifuge. After washing, cells were stained with a fluorescence antibody cocktail (containing FITC-αCD11c, APC-αCD80, PE-αCD86, PE/Cyanine7-αMHC-I, and PerCP/Cyanine5.5-αMHC-II). After incubation, cells were washed, resuspended in PBS, and measured by flow cytometry.

In vivo antitumor efficacy of combo therapy

All animal experiments were approved by the Animal Care and Use Committee of Soochow University and conducted according to the Guidelines for the Care and Use of Experimental Animals. For human-derived mCRPC (LNCaP) xenograft mice, tumor cells were subcutaneously injected into the right upper back of male NCG mice. Once the tumor volume reached approximately 200 mm^3, 200 μL of ^{177}Lu-S1R/PSMA-P (100 μCi) was administered (i.v.) and this day was regarded as day 0. For combination groups, 24 h after TRT administration, PAPRi (40 mg/kg) or ATMi (10 mg/kg) was administered (p.o.). DDRi was given daily from day 1 for 9 successive days. Each treatment group consisted of four mice ($n = 4$).

For immune-competent RM-1-hPSMA murine prostate cancer model, tumor cells were subcutaneously injected into the right upper back of male C57BL/6J mice. ^{177}Lu-S1R/PSMA-P (100 μCi) was administered (i.v.) at tumor volume of 100–200 mm^3 (denoted as day 0). For combination groups, 24 h after TRT administration, PAPRi (40 mg/kg) or ATMi (10 mg/kg) was administered (p.o.). αCTLA-4 (20 μg) was injected (i.v.) 48 h after TRT. DDRi was administered on days 1, 2, 4, 5, 7, 8, 10 and 11 (8 doses in total), while αCTLA-4 was administered on days 2, 5, 10 and 13 (4 doses in total). Each treatment group consisted of seven mice ($n = 7$). Tumor volume and body weight of mice were measured every 3 days. Mice were considered dead when tumor volume exceeded 2000 mm^3 or body weight loss exceeded 15%.

Immune analyses of TME and systemic immune response in combo therapy

For immune analyses, RM-1-hPSMA mice treated with combo therapy as above were sacrificed on day 14. Tumors were harvested, minced, and passed through a filter, followed by red blood cell lysis and washing to obtain a single-cell suspension. Cells were treated with Zombie NIR™ Fixable Viability Kit to distinguish live and dead cells. After washing, cells were blocked (αCD16/32) and stained with fluorescent antibodies. For intracellular protein staining, surface antigen staining was performed, followed by fixation, permeabilization using the FoxP3/Transcription Factor Staining Buffer Kit, and subsequent staining of intracellular proteins. Flow cytometry was performed, and data were analyzed using FlowJo V10 software ($n = 4$). The following cell populations were analyzed: $CD4^+$ T ($CD45^+CD3^+CD4^+$), $CD8^+$ T ($CD45^+CD3^+CD8^+$), Th1 cells ($CD45^+CD3^+CD4^+IFN\text{-}\gamma^+TNF\text{-}\alpha^+$), cytotoxic T lymphocytes ($CD45^+CD3^+CD8^+GZMB^+Perforin^+$ and $CD45^+CD3^+CD8^+IFN\text{-}\gamma^+TNF\text{-}\alpha^+$), $CD4^+$ regulatory T cells (Tregs, $CD45^+CD3^+CD4^+CD25^+FoxP3^+$), natural killer (NK, $CD45^+NKG2D^+NK1.1^+CD107a^+$) cells, tumor-associated macrophages (TAMs, $CD45^+CD11b^+F4/80^+CD86^+CD206^+$), and myeloid-derived suppressor cells (MDSCs, $CD45^+CD11b^+Gr\text{-}1^+$).

For systemic immune analyses, peripheral blood, spleen and peritumoral lymph node were collected from mice on day 14 post-treatment, and the subsequent steps followed the same procedure as for TME analyses.

Statistical analyses

All data are presented as mean ± standard deviation. Data processing and significance analyses were performed using GraphPad Prism 9. Statistical significance was assessed using one-way analyses of variance (ANOVA). Kaplan-Meier survival curves were plotted and compared using the log-rank test. Significance levels are indicated as follows: * $p < 0.05$, ** $p < 0.01$, *** $p < 0.001$, and **** $p < 0.0001$.

Results

DDRi enhances the antitumor efficacy of TRT in human LNCaP cells and xenografts in mice

We firstly evaluated the effects of PARPi and ATMi on sensitizing TRT with ^{177}Lu-S1R/PSMA-P in human LNCaP cells and xenografts in mice. The cell viability assays revealed that a low concentration of PARPi (2 μM) and ATMi (10 nM) significantly enhanced the cytotoxic effect of TRT to LNCaP cells (Fig. 1a, b). LNCaP tumor-bearing mice was established by subcutaneously injected tumor cells (Fig.**S1**). The in vivo treatment started at tumor volume of 150–250 mm^3 by intravenously injecting 100 μCi ^{177}Lu-S1R/PSMA-P and daily oral administration of PARPi (40 mg/kg) or ATMi (10 mg/kg) on the second day and for 9 successive days (Fig. 1c). The results showed that both PARPi and ATMi had limited effects on tumor growth, and a single dose of ^{177}Lu-S1R/PSMA-P caused substantial tumor suppression (Fig. 1d, e). Notably, TRT combined with either PARPi or ATMi led to a continuous shrinkage of tumors, which was significantly more effective than TRT alone. It should further be noted that ATMi induced clearly more pronounced tumor shrinkage than PARPi (tumor volume on day 28: 23.12 ± 9.60 mm^3 *versus* 52.57 ± 17.05 mm^3). The mouse body weight remained stable during treatments (Fig. 1f), indicating that TRT-DDRi combo therapy is well tolerated.

DDRi boosts the antitumor effect of TRT in murine RM-1-hPSMA cells and tumors in mice

We further investigated the sensitizing effects of PARPi or ATMi on ^{177}Lu-S1R/PSMA-P in radiation-resistant murine RM-1-hPSMA prostate cancer cells and mouse models. RM-1-hPSMA exhibits high expression of human PSMA (hPSMA) (Fig. S2a, b). Figure 2a shows a strong radioresistance of RM-1-hPSMA cells, with survival rate exceeding 80% after 48 h of varying doses of TRT treatment. While PARPi and ATMi alone had minimal impact on cell viability (Fig. S2c, d), both PARPi and ATMi significantly enhanced the inhibitory effect of TRT (Fig. 2b, c). The in vivo efficacy studies were conducted in subcutaneous RM-1-hPSMA tumor models by oral administration of DDRi starting from one day later than TRT and giving two doses in three days and for a total of four cycles. TRT monotherapy at 100 μCi only mildly delayed tumor progression (Fig. 2e). Interestingly, combination with DDRi, in particular ATMi, significantly boosted tumor inhibition (Fig. 2e, f). In accordance, mice median survival time (MST) increased from 23 days for TRT monotherapy to 34 and 48 days for combo with PARPi and ATMi, respectively (Fig. 2g). TRT could be compromised by the high infiltration of Tregs within the TME [37]. We further investigated the effects of αCTLA-4 antibody, which might counteract Treg-mediated suppression of antigen presentation and promote the activation and proliferation of Th1 cells [38–40]. Thrillingly, although the tumor-suppressive effects differed greatly for TRT-PARPi and TRT-ATMi combo, excellent treatment outcomes were accomplished for both when adding αCTLA-4, achieving complete tumor remission in 57% and 71% of mice, respectively (Fig. 2g). Throughout the treatment, body weight remained stable across all experimental groups (Fig. 2h), providing evidence of good safety.

ATMi effectively reverses radioresistance

DDRi, in particular ATMi, enables effective radio-sensitization of prostate tumor cells in vitro and tumors in vivo. Hereafter, we investigated the mechanisms by which DDRi sensitizes RM-1-hPSMA cells to TRT. Of note, both PARPi and ATMi markedly enhanced TRT-induced DNA fragmentation, as shown by the increased intensity of TUNEL fluorescent signals bound to fragmented DNA (Fig. 3a, Fig. S3a). Histone H2AX is phosphorylated to γ-H2AX upon the occurrence of DSB, rapidly localizing to damage sites. Consequently, γ-H2AX serves as a marker for DSB and acts as a platform to recruit DNA repair proteins, activating DSB repair pathways [41]. CLSM and flow cytometry results confirmed that TRT-DDRi treatment significantly induced DSB, as evidenced by a marked increase in γ-H2AX expression (Fig. 3b–d). However, compared to TRT-PARPi combo, γ-H2AX upregulation was less pronounced in the TRT-ATMi combo. This is because ATM, as an upstream kinase of H2AX phosphorylation, is inhibited by ATMi, thereby reducing γ-H2AX levels. This inhibition impairs γ-H2AX-mediated DSB repair and exacerbates tumor cell death [35]. The apoptosis assays showed that the proportion of apoptotic cells increased from 16.9 to 34.9% and 67.9% by combining with PARPi and ATMi, respectively (Fig. 3e, f, Fig. S3b, c). TRT combined with PARPi was shown to induce substantial G2/M phase arrest (79.6%) while combination with ATMi resulted in only a modest increase in the G2/M phase population (54.4%) (Fig. 3g, h, Fig. S3d, e). As a result, tumor cells treated with TRT-ATMi were forced to rely on non-homologous end joining (NHEJ) for DSB repair, which leads to misrepair and extensive apoptosis. Hence, DDRi in particular ATMi significantly amplifies TRT-induced DNA damage and reverses radioresistance by inhibiting DSB repair.

RNA-seq analyses of RM-1-hPSMA cells treated with TRT-DDRi

The effects of DDRi on TRT were investigated by RNA sequencing (RNA-Seq). The volcano plot of differentially

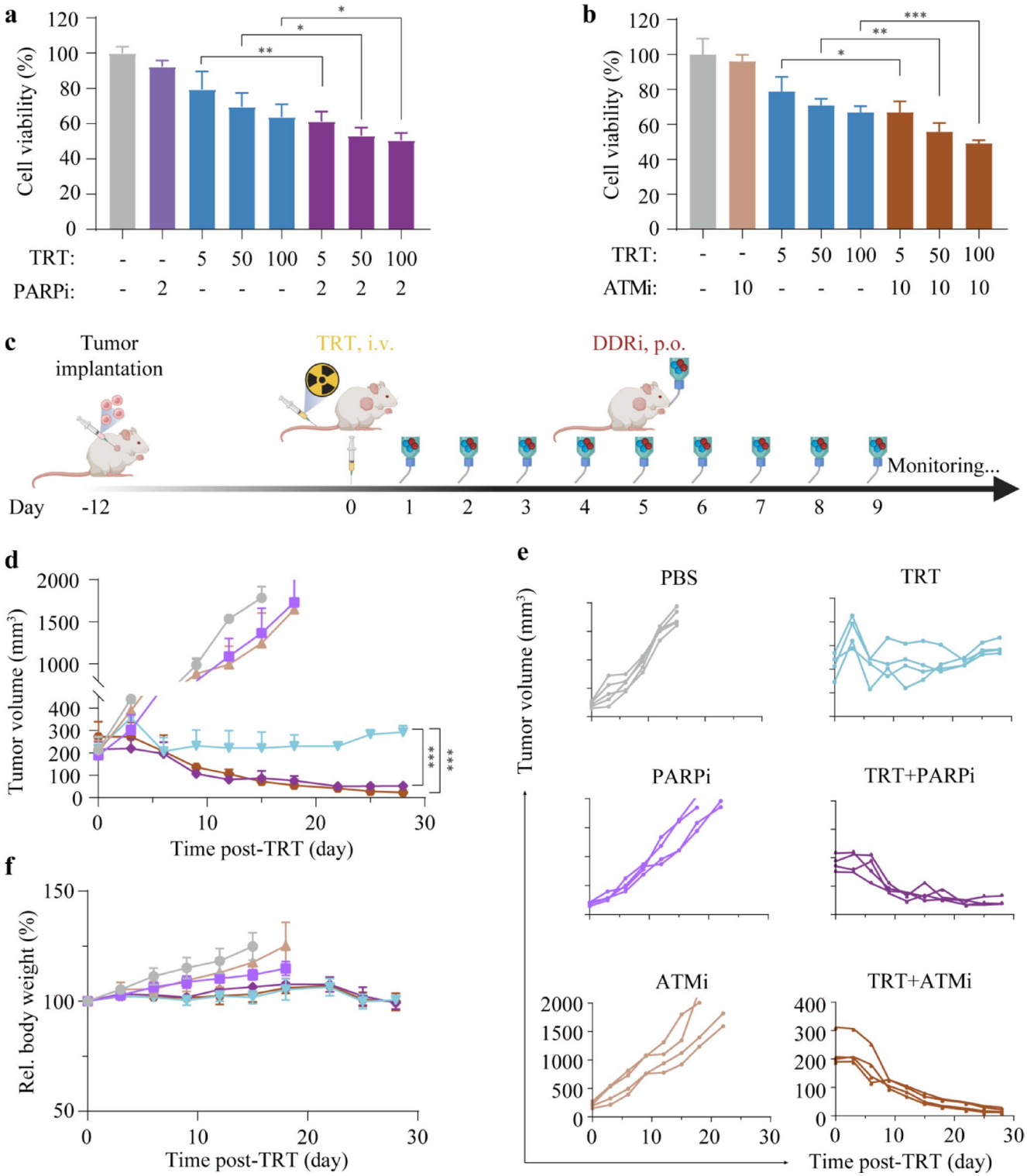

Fig. 1 PARPi and ATMi enhance TRT of human LNCaP prostate cells and tumor models. Viability of LNCaP cells following ^{177}Lu-S1R/PSMA-P treatment combined with (a) PARPi (2 µM) or (b) ATMi (10 nM) for 48 h. (c) The in vivo treatment scheme with TRT (100 µCi) in combination with either PARPi (40 mg/kg) or ATMi (10 mg/kg) toward LNCaP-bearing mice for Fig. 1d-f ($n = 4$). (d) Tumor growth curves, (e) individual tumor growth curves and (f) relative body weights of mice. * $p < 0.05$, ** $p < 0.01$, *** $p < 0.001$

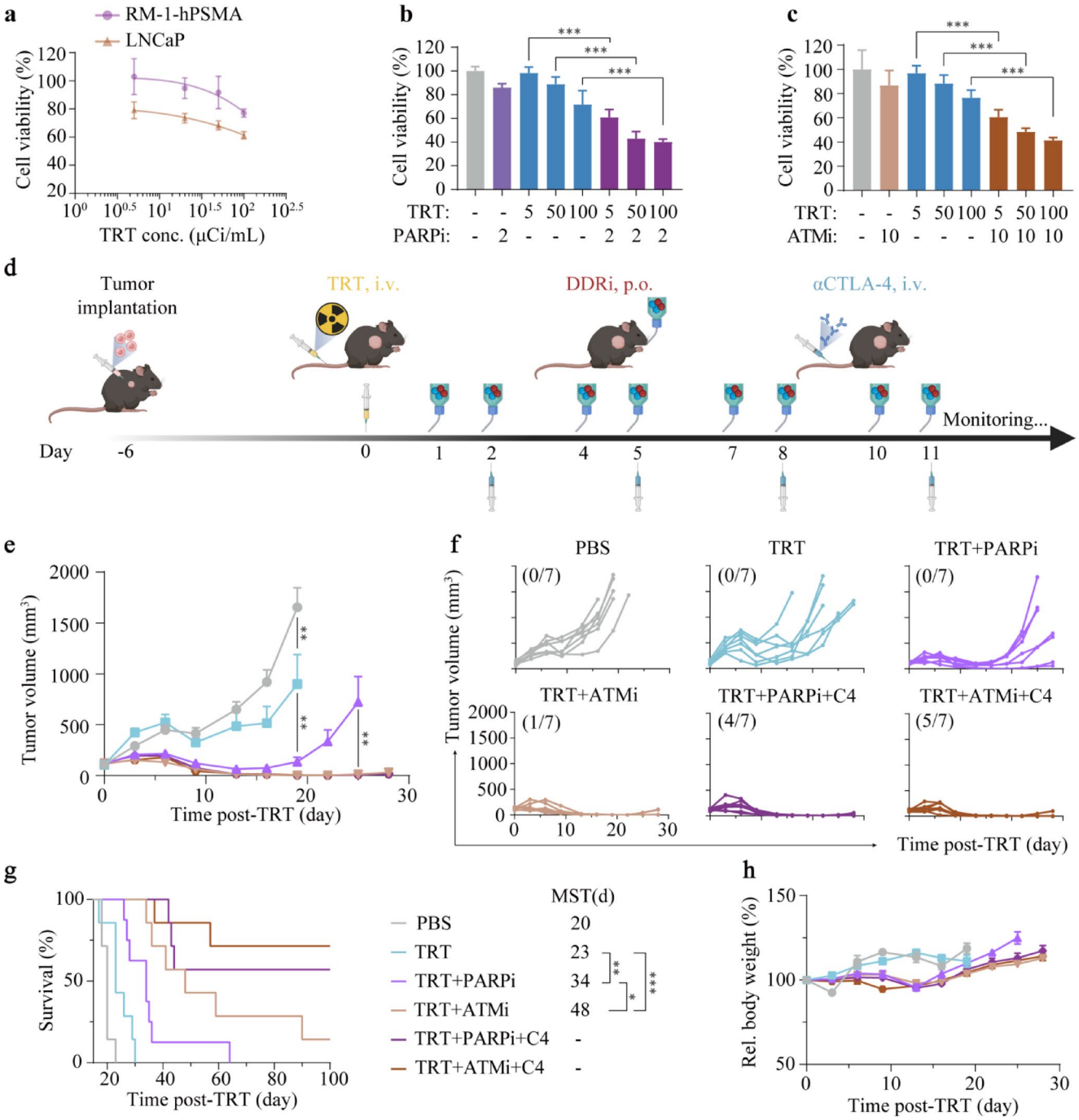

Fig. 2 PARPi and ATMi enhance TRT of murine RM-1-hPSMA prostate tumor model. (a) Cell viability of RM-1-hPSMA and LNCaP cells after 48 h of TRT treatment at increasing doses ($n = 6$). Cell viability of RM-1-hPSMA cells following 48 h treatment with increasing doses of TRT combined with (b) PARPi (2 μM) or (c) ATMi (10 nM). (d) The in vivo treatment scheme with TRT (100 μCi), in combination with either PARPi (40 mg/kg) or ATMi (10 mg/kg), and with or without C4 (αCTLA-4, 20 μg) for Fig. 2e, g, h ($n = 7$). (e) Tumor growth curves. (f) Individual tumor growth curves. (g) Kaplan-Meier survival curves and median survival time (MST). (h) Relative body weights of RM-1-hPSMA-bearing mice with different treaments. * $p < 0.05$, ** $p < 0.01$, *** $p < 0.001$

expressed genes (DEGs) revealed that TRT caused 342 upregulated and 173 downregulated genes suggesting resistance to apoptosis and immune escape (Fig. 4a). In comparison, TRT combined with PARPi and ATMi induced DEGs indicating inhibited DDR, exacerbated radiation stress, and enhanced immune responses (Fig. 4b, S4a). Gene ontology (GO) enrichment analyses displayed that TRT predominantly affected G protein-coupled receptor signaling

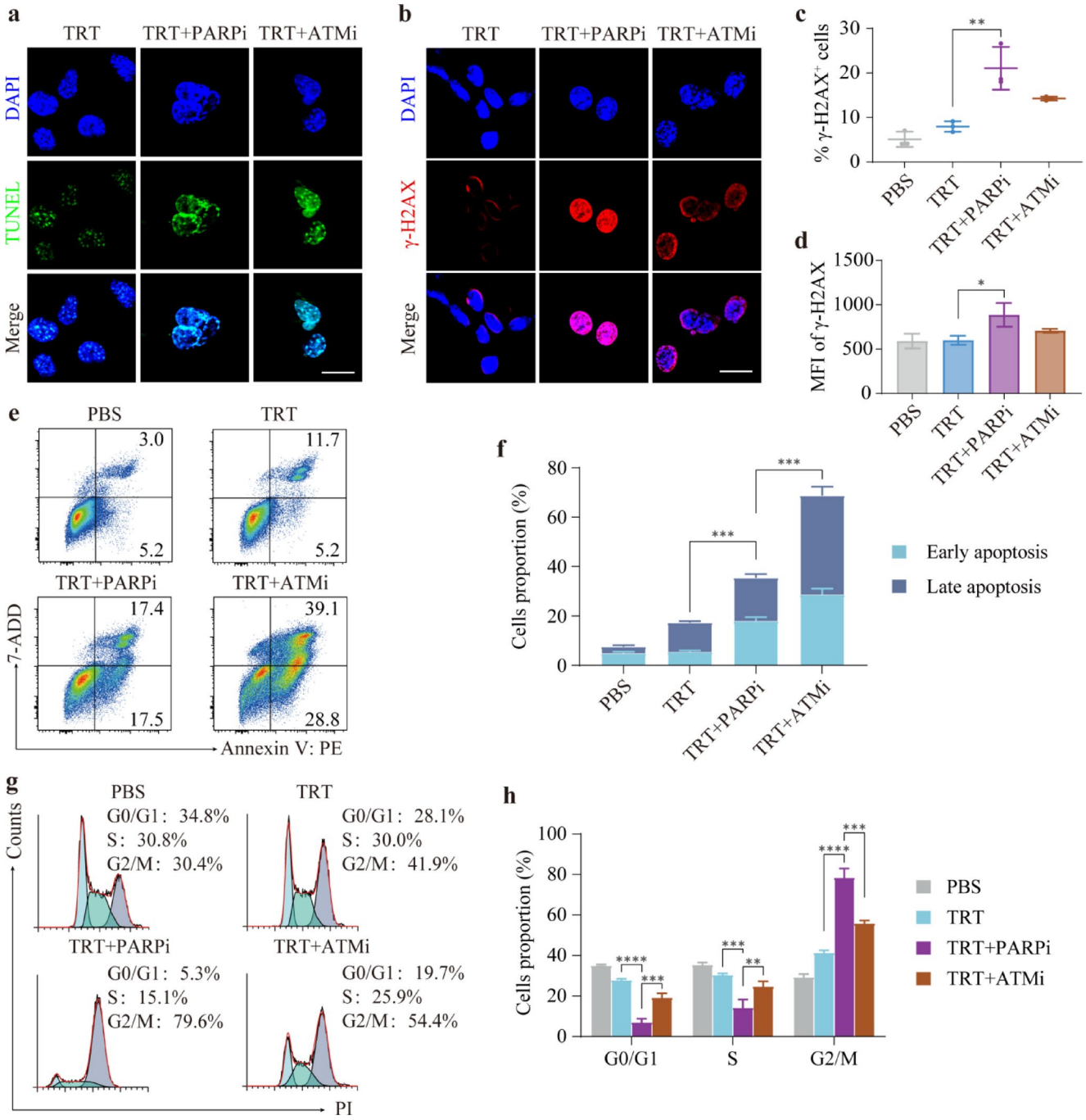

Fig. 3 Effects of PARPi (2 μM) or ATMi (10 nM) on TRT (^{177}Lu-S1R/PSMA-P, 50 μCi/mL, 48 h) of RM-1-hPSMA cells. Confocal microscopy images showing (a) TUNEL staining and (b) γ-H2AX expression in RM-1-hPSMA cells (scale bar: 10 μm). Flow cytometry analyses of (c) γ-H2AX$^+$ cells and (d) γ-H2AX expression intensity ($n = 3$). Apoptosis in RM-1-hPSMA cells, shown as (e) representative flow cytometry plots and (f) quantification ($n = 3$). Cell cycle analyses of RM-1-hPSMA cells treated with TRT combined with PARPi or ATMi at 24 h, represented by (g) flow cytometry plots and (h) quantification ($n = 3$). * $p < 0.05$, ** $p < 0.01$, *** $p < 0.001$, **** $p < 0.0001$

pathways and inflammation-related pathways but failed to activate key antitumor immune mechanisms, potentially leading to immune escape and radioresistance (Fig. S4b). In contrast, TRT combined with PARPi significantly enriched pathways related to immune responses, cell adhesion, and inflammation regulation, indicating enhanced DDR, TME remodeling, and immune cell migration (Fig. 4c). ATMi combination therapy further enriched acute-phase and defense response pathways, suggesting severe radiation-induced damage triggering robust stress responses (Fig.

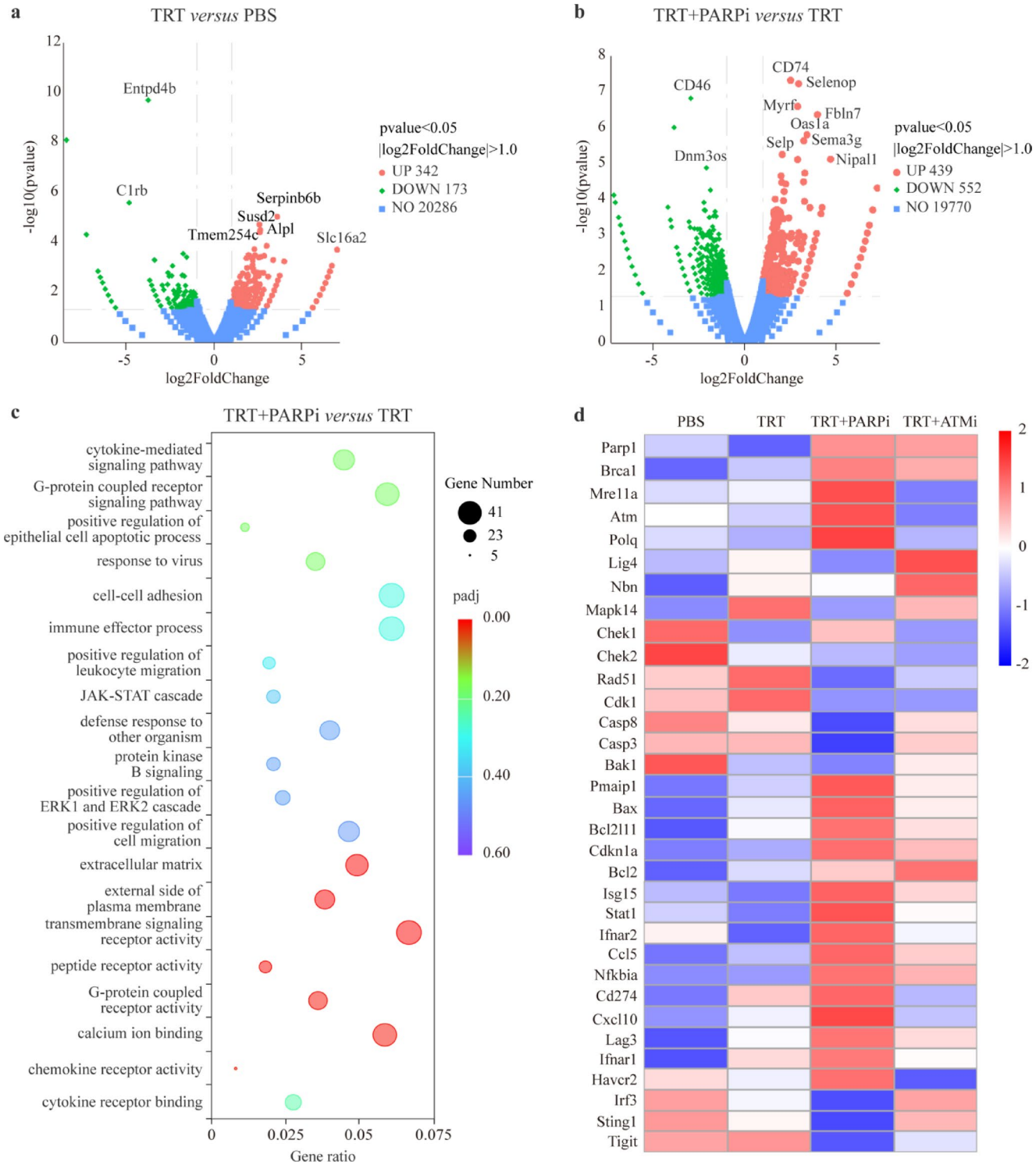

Fig. 4 RNA-seq analyses of RM-1-hPSMA cells following TRT (^{177}Lu-S1R/PSMA-P, 50 µCi/mL), with either PARPi (2 µM) or ATMi (10 nM) treatment. (a) Volcano plot showing differentially expressed genes (DEGs) in RM-1-hPSMA cells treated with TRT versus PBS control. (b) Volcano plot and (c) GO enrichment analyses of DEGs in RM-1-hPSMA cells treated with TRT + PARPi versus TRT alone. Adjusted p-values (padj) were calculated using the Benjamini-Hochberg method to control the false discovery rate. (d) Heatmap analyses of DEGs in RM-1-hPSMA cells subjected to various treatments. Gene expression values were calculated as $\log_2$(FPKM + 1) and normalized using Z-score transformation (zero-mean normalization). Color intensity represents standardized expression levels across samples (red indicates upregulation, blue indicates downregulation)

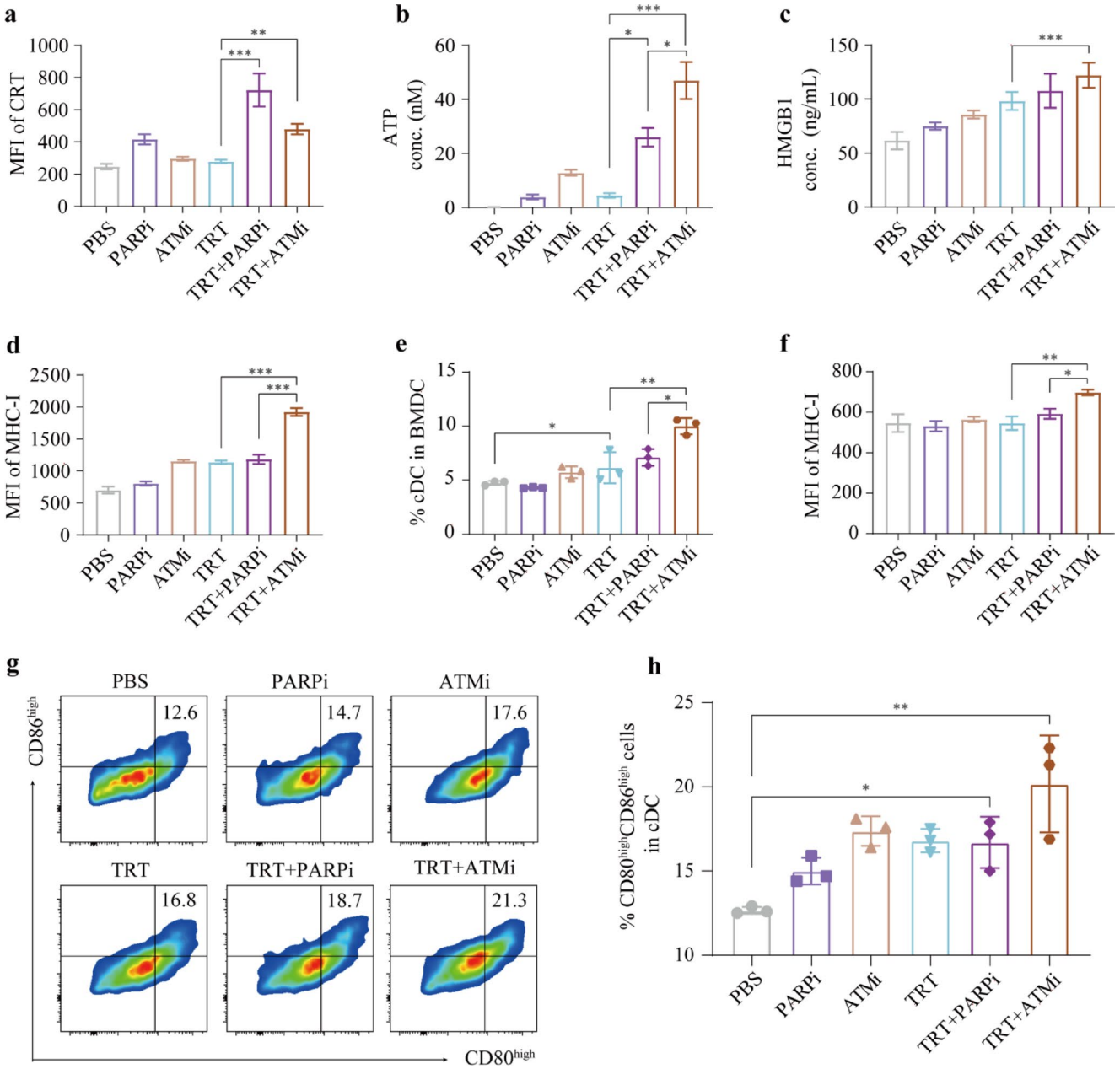

Fig. 5 Effects of TRT (^{177}Lu-S1R/PSMA-P, 50 μCi/mL) combined with PARPi (2 μM) or ATMi (10 nM) on the (a) CRT expression, (b) ATP secretion, (c) HMGB1 release, and (d) MHC-I expression within RM-1-hPSMA cells ($n = 3$). (e) Proportion of cDCs ($CD11c^+MHC\text{-}II^+$) and (f) MHC-I expression of BMDCs after treatment with tumor cells damaged by TRT combined with PARPi or ATMi ($n = 3$). (g) Representative flow cytometry plots and (h) quantitative analyses of the proportion of cDCs with high costimulatory molecule expressing ($CD80^{high}CD86^{high}$) in total cDCs ($n = 3$). * $p < 0.05$, ** $p < 0.01$, *** $p < 0.001$

S4c). Heatmap analyses highlighted DEGs in pathways identified through GO enrichment (Fig. 4d). Compared to TRT alone, PARPi combination markedly upregulated DDR-related genes, reflecting active repair of SSB and DSB. Upregulation of pro-apoptotic factors (Pmaip1, Bax, Bcl2l11) indicated intensified DNA damage. In contrast, ATMi significantly downregulated DSB repair-related genes, confirming inhibition of homologous recombination (HR) repair, while upregulation of Lig4 indicated a shift toward NHEJ. The significant downregulation of cell cycle checkpoint genes (Chek1, Chek2, Cdk1) suggested checkpoint dysfunction, enhancing TRT-induced radiotoxicity by impairing DSB repair. Importantly, TRT combined with PARPi or ATMi significantly activated the type I interferon signaling pathway, likely promoting infiltration of anti-tumor effector cells (T cells and NK cells) into the TME. PARPi combination also upregulated immune suppressive genes, potentially leading to T cell exhaustion and immune

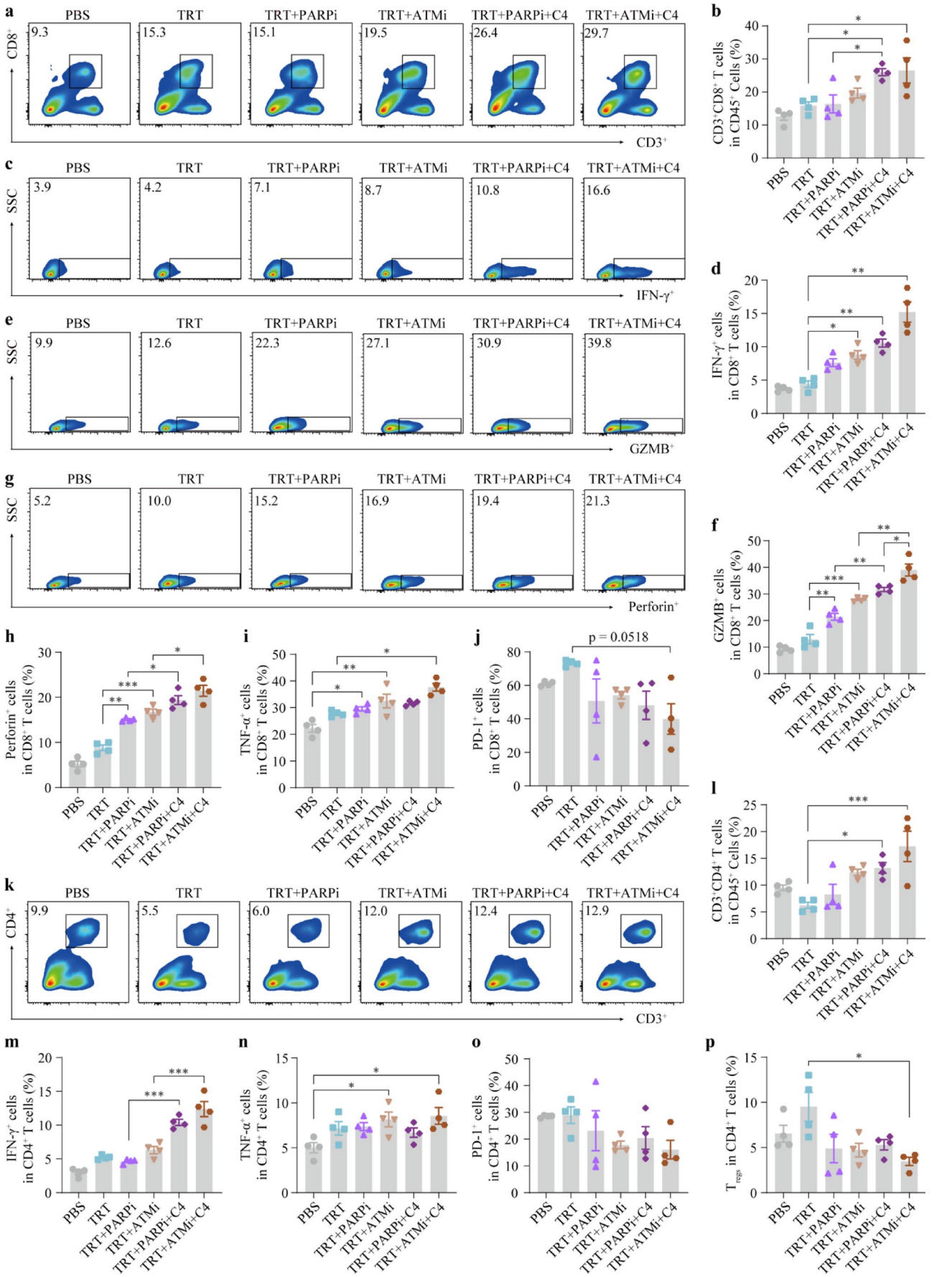
a
PBS
TRT
TRT+PARPi
TRT+ATMi
TRT+PARPi+C4
TRT+ATMi+C4
CD8+
9.3
15.3
15.1
19.5
26.4
29.7
CD3+
b
CD3+CD8+ T cells in CD45+ Cells (%)
c
SSC
3.9
4.2
7.1
8.7
10.8
16.6
IFN-γ+
d
IFN-γ+ cells in CD8+ T cells (%)
e
SSC
9.9
12.6
22.3
27.1
30.9
39.8
GZMB+
f
GZMB+ cells in CD8+ T cells (%)
g
SSC
5.2
10.0
15.2
16.9
19.4
21.3
Perforin+
h
Perforin+ cells in CD8+ T cells (%)
i
TNF-α+ cells in CD8+ T cells (%)
j
p = 0.0518
PD-1+ cells in CD8+ T cells (%)
k
CD4+
9.9
5.5
6.0
12.0
12.4
12.9
CD3+
l
CD3+CD4+ T cells in CD45+ Cells (%)
m
IFN-γ+ cells in CD4+ T cells (%)
n
TNF-α+ cells in CD4+ T cells (%)
o
PD-1+ cells in CD4+ T cells (%)
p
Tregs in CD4+ T cells (%)

Fig. 6 Immunological analyses of the TME in murine RM-1-hPSMA prostate tumor models treated with TRT (^{177}Lu-S1R/PSMA-P, 100 μCi) combined with PARPi (40 mg/kg) or ATMi (10 mg/kg), and further with C4 (αCTLA-4, 20 μg) on day 14 ($n = 4$). (a) Representative flow cytometry plots and (b) quantification of CD8$^+$ T cell percentages in CD45$^+$ cells. (c) Representative flow cytometry plots and (d) quantification of IFN-γ$^+$ cells among CD8$^+$ T cells. (e) Representative flow cytometry plots and (f) quantification of GZMB$^+$ cells among CD8$^+$ T cells. (g) Representative flow cytometry plots and (h) quantification of perforin$^+$ cells among CD8$^+$ T cells. (i) Proportions of TNF-α$^+$ cells among CD8$^+$ T cells. (j) Proportions of exhausted CD8$^+$ T cells (PD-1$^+$) among CD8$^+$ T cells. (k) Representative flow cytometry plots and (l) quantification of CD4$^+$ T cell percentages in CD45$^+$ cells.Proportions of (m) IFN-γ$^+$ cells, (n) TNF-α$^+$ cells, (o) exhausted CD4$^+$ T cells (PD-1$^+$), and (p) Tregs (CD25$^+$FoxP3$^+$ cells) among CD4$^+$ T cells. * $p < 0.05$, ** $p < 0.01$, *** $p < 0.001$

escape. In contrast, ATMi combination strongly activated the STING pathway and suppressed immune suppressive genes, further enhancing antitumor immune responses. The above results demonstrate that DDRi significantly amplifies TRT-induced DNA damage and antitumor immunity, and ATMi is superior to PARPi by effectively inhibiting DSB repair and reducing immune escape, hence overcoming radioresistance.

ATMi induces immunogenic cell death and remodels TME

We further investigated how DDRi affects TME. Figure 5a–c reveals that TRT combined with PARPi or ATMi markedly elevated the levels of calreticulin (CRT), adenosine triphosphate (ATP), and high-mobility group box 1 (HMGB1), suggesting that RM-1-hPSMA cells are subject to immunogenic cell death (ICD). Moreover, ATMi further increased TRT-upregulated major histocompatibility complex class I (MHC-I) (Fig. 5d), which might enhance CD8$^+$ T cell recognition and cytotoxicity [42]. Classical dendritic cells (cDCs) play a pivotal role in bridging innate and adaptive immunity. While conditioned media from TRT-treated RM-1-hPSMA cells were capable of promoting the differentiation of bone marrow-derived dendritic cells (BMDCs) into cDCs and upregulating the expression of costimulatory molecules, TRT-ATMi treatment not only further increased the proportion of cDCs (9.99%) and cDCs with high costimulatory molecule expressing (21.3%) but also significantly enhanced MHC-I expression on cDCs (Fig. 5e–h). These findings suggest that TRT combined with DDRi, particularly ATMi, may remodel the immunosuppressive TME and enhance adaptive immune responses by promoting DC-mediated antigen presentation, robustly activating antitumor immune responses.

TRT-DDRi-αCTLA-4 reverses suppressive tumor microenvironment and induces durable systemic immune responses

The flow cytometry and immunofluorescence analyses showed that unlike PARPi, ATMi induced a notable increase in CD8$^+$ T cell infiltration in the TME, and addition of αCTLA-4 boosted CD8$^+$ T cell infiltration for both TRT-PARPi and TRT-ATMi combinations (Fig. 6a, b, Fig. S5). The proportion of cytotoxic CD8$^+$ T cells, characterized by elevated secretion of IFN-γ, TNF-α, granzyme B, and perforin, also increased significantly (Fig. 6c–i). These findings indicate that TRT-DDRi-αCTLA-4 not only expands CD8$^+$ T cells but also enhances their cytotoxic function. DDRi-αCTLA-4 also significantly reversed TRT-induced CD8$^+$ T cell exhaustion (Fig. 6j) and markedly upregulated MHC-I expression on tumor cells (Fig. S6a). CD4$^+$ T cells, key regulators of CD8$^+$ T cell-mediated antitumor responses [43], exhibited significantly increased infiltration only under TRT-DDRi-αCTLA-4 combo therapy (Fig. 6k, l). Notably, the proportion of Th1 cells increased significantly, accompanied by elevated secretion of IFN-γ and TNF-α (Fig. 6m, n). These changes promoted cytotoxic CD8$^+$ T cell activation and proliferation, while also reversing CD4$^+$ T cell exhaustion (Fig. 6o). TRT combined with DDRi, especially ATMi, significantly reduced the accumulation of tumor infiltrating immunosuppressive cells, such as Tregs, MDSCs, and CD206$^+$ TAMs, which are major contributors to radioresistance (Fig. 6p, S6b–d). Of note, TRT-AMTi-αCTLA-4 resulted in not only further reduction of immunosuppressive cells but also significantly increased both the number and cytotoxicity (CD107a$^+$) of activated NK cells (NK1.1$^+$) (Fig. S6e, f), enhancing the innate immune response against tumor cells with low MHC-I expression.

On day 14, systemic immune responses were analyzed. TRT-DDRi-αCTLA-4 combo therapy markedly increased the proportions of CD4$^+$ and CD8$^+$ T cells in the spleen, peripheral blood, and peritumoral lymph nodes (Fig. 7a, b, S7a–d), indicating a magnified effect of activation of systemic immunity by αCTLA-4. Serum levels of IFN-γ and TNF-α were significantly elevated across all combination treatment groups (Fig. 7c, d), further indicating systemic immune activation. As the largest secondary lymphoid organ, the spleen supports systemic immune responses. Phenotypic analyses of spleen immune cells showed marked increases in early activation markers (CD25$^+$) and intermediate activation markers (CD69$^+$) on CD8$^+$ T cells exclusively in the αCTLA-4 combination group (Fig. 7e, f). Cytotoxic CD8$^+$ T cells exhibited enhanced functionality, consistent with observations in the TME (Fig. 7g–j) and correlated strongly with αCTLA-4-induced CD4$^+$ T cell differentiation into Th1 cells (Fig. 7k, l). The proportion of Tregs

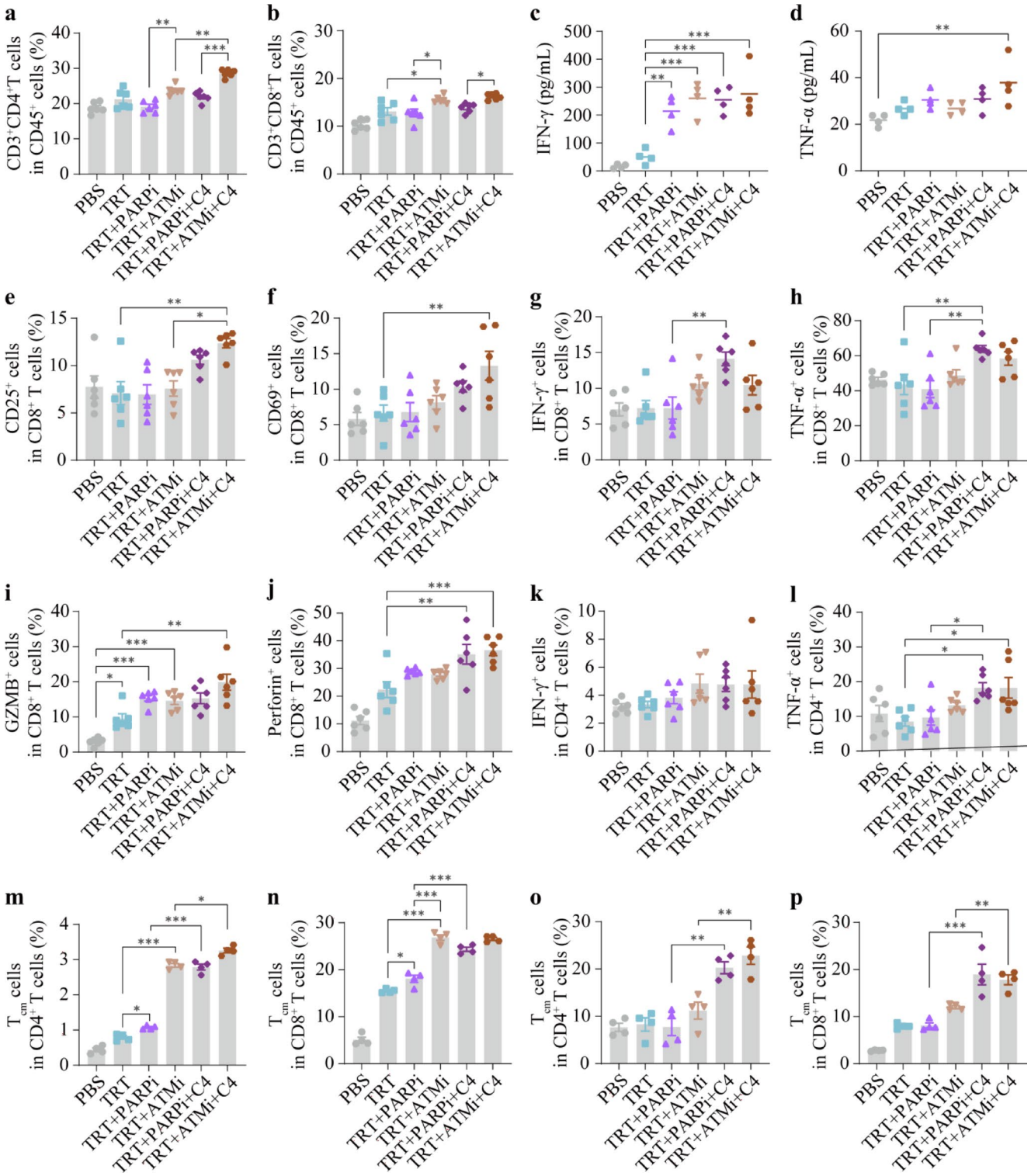

Fig. 7 Analyses of systemic immune response in murine RM-1-hPSMA prostate tumor models treated with TRT (^{177}Lu-S1R/PSMA-P, 100 μCi) combined with PARPi (40 mg/kg), or ATMi (10 mg/kg), and further with C4 (αCTLA-4, 20 μg) on day 14. (a) Proportions of CD4$^+$ T cells and (b) CD8$^+$ T cells in CD45 +T cells in the spleen (n = 6). (c) Serum levels of IFN-γ and (d) TNF-α (n = 4). (e) Proportions of early activation (CD25$^+$) and (f) mid-stage activation (CD69$^+$) in CD8$^+$ T cells (n = 6). Proportions of (g) GZMB$^+$, (h) perforin$^+$, (i) IFN-γ$^+$, and (j) TNF-α$^+$ cells among CD8$^+$ T cells (n = 6). (k) Proportions of IFN-γ$^+$ and (l) TNF-α$^+$ cells among CD4$^+$ T cells in the spleen (n = 6). Proportions of (m) CD4$^+$ and (n) CD8$^+$ central memory T (Tcm) cells (CD62L$^+$CD44$^+$) in the spleen on day 21 (n = 4). Proportions of (o) CD4$^+$ and (p) CD8$^+$ Tcm cells in peripheral blood on day 21 (n = 4). * p < 0.05, ** p < 0.01, *** p < 0.001

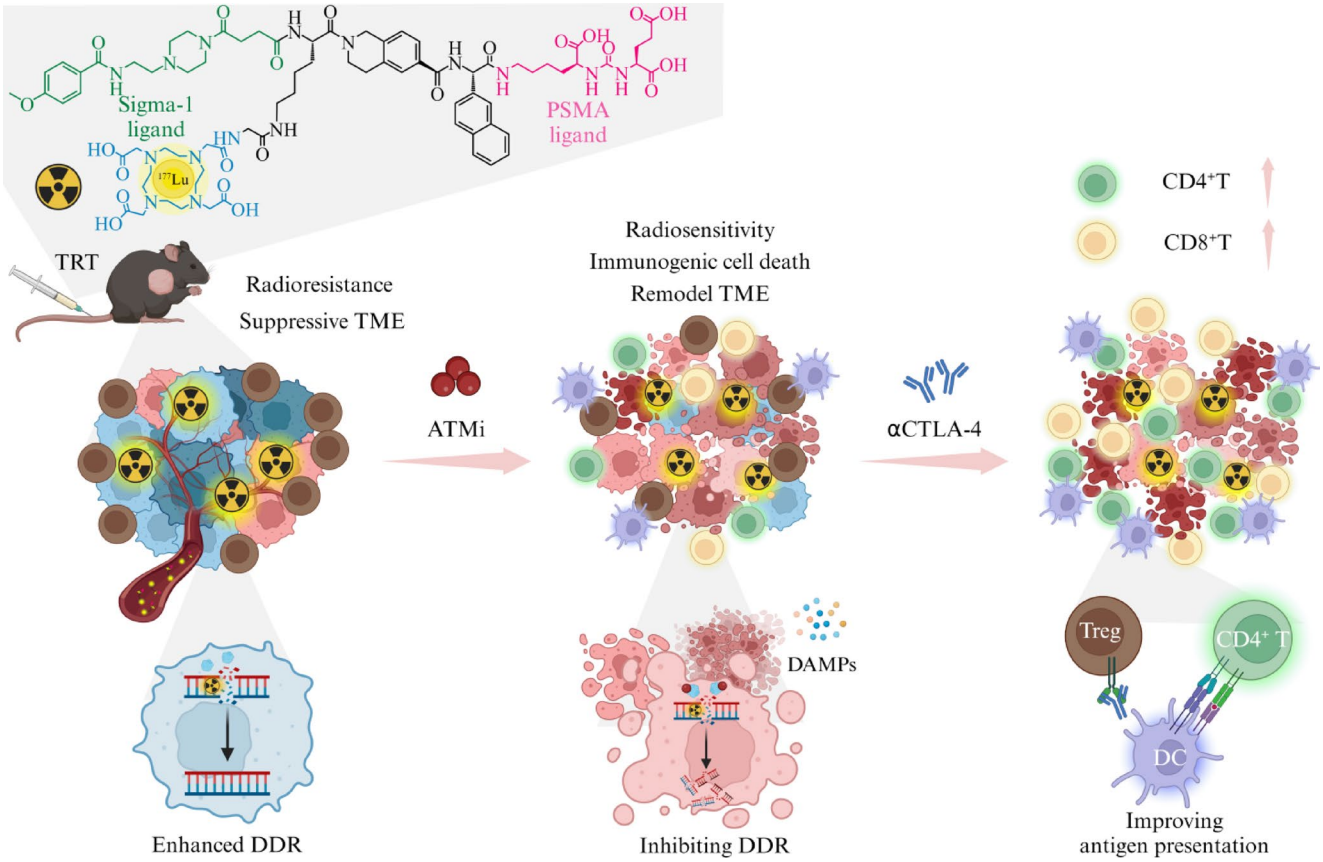

Scheme 1 Schematic illustration of DNA damage repair inhibitor, ATM inhibitor (ATMi), for targeted radionuclide therapy and immunotherapy of malignant murine RM-1-hPSMA prostate cancer model with αCTLA-4 antibody. ATMi amplifies TRT-induced DNA damage and immunogenic cell death in tumor cells, and reshapes the suppressive tumor microenvironment, which combined with αCTLA-4 antibody induces potent and long-lasting anticancer immunity

was significantly reduced in the αCTLA-4 combination group (Fig. S7e, f), while TRT combined with either PARPi or ATMi decreased MDSCs and macrophages (predominantly CD206$^+$) by approximately 20% (Fig. S7g–i), all pointing to reduced immunosuppressive effects. Additionally, Activated NK cells were significantly enhanced, suggesting activation of innate immune responses (Fig. S7j–l). Furthermore, αCTLA-4 enhanced systemic immunity by inhibiting Tregs and promoting Th1 cells activity. On day 21, the analyses of central memory T cells (Tcm) in the spleen and peripheral blood revealed significant increases in CD4$^+$ Tcm and CD8$^+$ Tcm proportions in the TRT-DDRi-αCTLA-4 group (Fig. 7m–p). This suggests that αCTLA-4 plays a critical role in promoting adaptive immune memory, a key factor contributing to complete tumor remission.

Discussion

TRT targeting PSMA has emerged as a promising therapeutic strategy for patients with mCRPC. However, the clinical efficacy of TRT is limited by intrinsic tumor resistance mechanisms, including enhanced DDR and immunosuppressive TME. Our study demonstrates that DDRi, particularly ATMi, potentiates the efficacy of TRT by blocking the repair of TRT-induced DNA damage and promoting tumor cell death (Scheme 1). Beyond direct cytotoxic effects, combining TRT with DDRi effectively activates CD8$^+$ T cells, promoting their proliferation and function, while significantly reducing the proportion of immunosuppressive cells such as Tregs, thereby remodeling the TME and enhancing systemic immune responses. The addition of αCTLA-4 not only amplifies these effects but also stimulates CD4$^+$ T cell differentiation into Th1 cells and induces adaptive immune memory effect, strengthening immune surveillance. Our results further show that selection of DDRi critically influences the efficacy of TRT, in which ATMi outperforms PARPi. It has been reported that PARPi can enhance the antitumor effect of ^{177}Lu-DOTA-TOC in a small-cell lung cancer (SCLC) model with low SSTR2 expression [44]. In addition, several clinical trials are currently evaluating the safety and efficacy of combining TRT with PARPi, and preliminary results suggest promising therapeutic potential [45, 46]. It is interesting to note that while there are several

reports on influence of PARPi (inhibitor for single-strand DNA break), little work is done with inhibitors for double-strand DNA break repair. The finding that AMTi effectively reverses radioresistance and boosts anticancer immune response may greatly broaden the TRT for different tumors.

Conclusion

We have demonstrated that DNA damage repair inhibitors, in particular ATM inhibitor (ATMi), effectively boost TRT and immunotherapy of malignant murine prostate cancer, by reversing radioresistance, inducing immunogenic cell death, and reshaping the suppressive tumor microenvironment. It is remarkable that TRT-ATMi-αCTLA-4 induces robust and long-lasting adaptive anti-tumor immunity, resulting in 71% mice complete tumor regression. ATMi-αCTLA-4 provides a novel strategy to address the radioresistance and immune suppression issues that account for the modest response rates in the clinical settings. TRT-ATMi-αCTLA-4 with a high tumor-specificity has a great potential for immunotherapy of mCRPC patients.

Supplementary Information The online version contains supplementary material available at https://doi.org/10.1007/s10495-025-02136-7.

Acknowledgements This work is supported by research grants from the National Natural Science Foundation of China (NSFC52233007). The authors thank Biorender.com for assisting with the illustrations (https://BioRender.com/s01f741).

Author contributions B.X. carried out the experiments, analyzed the data and drafted the paper; L.T. carried out half of the experiments and analyzed the data; J.S. contributed to animal experiments and data analysis; J.Y. contributed to methodology and data validation; F.M. provided resources and revised the manuscript; Z.Z. conceptualized, supervised the work and revised the manuscript. All authors have reviewed and approved the manuscript.

Data availability No datasets were generated or analysed during the current study.

Declarations

Competing interests The authors declare no competing interests.

References

1. Siegel RL, Giaquinto AN, Jemal A (2024) Cancer statistics. CA Cancer J Clin 74(2024):12–49. https://doi.org/10.3322/caac.21820
2. Rebello RJ, Oing C, Knudsen KE, Loeb S, Johnson DC, Reiter RE, Gillessen S, Van der Kwast T, Bristow RG (2021) Prostate cancer. Nat Rev Dis Primers 7:9. https://doi.org/10.1038/s41572-020-00243-0
3. Sandhu S, Moore CM, Chiong E, Beltran H, Bristow RG, Williams SG (2021) Prostate cancer. Lancet 398:1075–1090. https://doi.org/10.1016/S0140-6736(21)00950-8
4. Gandaglia G, Karakiewicz PI, Briganti A, Passoni NM, Schiffmann J, Trudeau V, Graefen M, Montorsi F, Sun M (2015) Impact of the site of metastases on survival in patients with metastatic prostate cancer. Eur Urol 68:325–334. https://doi.org/10.1016/j.eururo.2014.07.020
5. Cai M, Song X-L, Li X-A, Chen M, Guo J, Yang D-H, Chen Z, Zhao S-C (2023) Current therapy and drug resistance in metastatic castration-resistant prostate cancer. Drug Resist Updat 68:100962. https://doi.org/10.1016/j.drup.2023.100962
6. Sartor O, Bono Jd, Chi KN, Fizazi K, Herrmann K, Rahbar K, Tagawa ST, Nordquist LT, Vaishampayan N, El-Haddad G, Park CH, Beer TM, Armour A, Pérez-Contreras WJ, DeSilvio M, Kpamegan E, Gericke G, Messmann RA, Morris MJ, Krause BJ (2021) Lutetium-177–PSMA-617 for metastatic castration-resistant prostate cancer. N Engl J Med 385:1091–1103. https://doi.org/10.1056/NEJMoa2107322
7. Hope TA, Eiber M, Armstrong WR, Juarez R, Murthy V, Lawhn-Heath C, Behr SC, Zhang L, Barbato F, Ceci F, Farolfi A, Schwarzenböck SM, Unterrainer M, Zacho HD, Nguyen HG, Cooperberg MR, Carroll PR, Reiter RE, Holden S, Herrmann K, Zhu S, Fendler WP, Czernin J, Calais J (2021) Diagnostic accuracy of 68Ga-PSMA-11 PET for pelvic nodal metastasis detection prior to radical prostatectomy and pelvic lymph node dissection: a multicenter prospective phase 3 imaging trial. JAMA Oncol 7:1635–1642. https://doi.org/10.1001/jamaoncol.2021.3771
8. Aboagye EO, Barwick TD, Haberkorn U (2023) Radiotheranostics in oncology: making precision medicine possible. CA Cancer J Clin 73:255–274. https://doi.org/10.3322/caac.21768
9. Senior M (2024) Precision radiation opens a new window on cancer therapy. Nat Biotechnol 42:1003–1008. https://doi.org/10.1038/s41587-024-02295-z
10. Sun J, Huangfu Z, Yang J, Wang G, Hu K, Gao M, Zhong Z (2022) Imaging-guided targeted radionuclide tumor therapy: from concept to clinical translation. Adv Drug Deliv Rev 190:114538. https://doi.org/10.1016/j.addr.2022.114538
11. Kuo H-T, Lin K-S, Zhang Z, Uribe CF, Merkens H, Zhang C, Bénard F (2021) 177Lu-labeled albumin-binder–conjugated PSMA-targeting agents with extremely high tumor uptake and enhanced tumor-to-kidney absorbed dose ratio. J Nucl Med 62:521–527. https://doi.org/10.2967/jnumed.120.250738
12. Xu M, Zhang P, Ding J, Chen J, Huo L, Liu Z (2022) Albumin binder–conjugated fibroblast activation protein inhibitor radiopharmaceuticals for cancer therapy. J Nucl Med 63:952–958. https://doi.org/10.2967/jnumed.121.262533
13. Wen X, Xu P, Zeng X, Liu J, Du C, Zeng X, Cheng X, Wang X, Liang Y, Zhao T, Yang H, Li H, Meng L, Fang J, Liu H, Zhou Z, Zhang J, Zhang X, Guo Z, Chen X (2023) Development of [177Lu]Lu-LNC1003 for radioligand therapy of prostate cancer with a moderate level of PSMA expression. Eur J Nucl Med Mol Imaging 50:2846–2860. https://doi.org/10.1007/s00259-023-06229-w
14. Cui X-Y, Li Z, Kong Z, Liu Y, Meng H, Wen Z, Wang C, Chen J, Xu M, Li Y, Gao J, Zhu W, Hao Z, Huo L, Liu S, Yang Z, Liu Z (2024) Covalent targeted radioligands potentiate radionuclide therapy. Nature 630:206–213. https://doi.org/10.1038/s41586-024-07461-6
15. Huangfu Z, Yang J, Sun J, Xu B, Tao L, Wu J, Wang F, Wang G, Meng F, Zhong Z (2024) Sigma-1 receptor dual-targeted peptide mediates superior radionuclide imaging and therapy of prostate cancer. J Control Release 375:767–775. https://doi.org/10.1016/j.jconrel.2024.09.040
16. Meyer C, Stuparu A, Lueckerath K, Calais J, Czernin J, Slavik R, Dahlbom M (2023) Tandem isotope therapy with (225)Ac- and

(177)Lu-PSMA-617 in a murine model of prostate cancer. J Nucl Med 64:1772–1778. https://doi.org/10.2967/jnumed.123.265433
17. Moradi Tuchayi A, Yadav S, Jiang F, Kim ST, Saelee RK, Morley A, Juarez R, Lawhn-Heath C, Wang Y, de Kouchkovsky I, Hope TA (2024) Real-world experience with (177)Lu-PSMA-617 radioligand therapy after food and drug administration approval. J Nucl Med 65:735–739. https://doi.org/10.2967/jnumed.123.266842
18. Satapathy S, Yadav MP, Ballal S, Sahoo RK, Bal C (2024) [177Lu]Lu-PSMA-617 as first-line systemic therapy in patients with metastatic castration-resistant prostate cancer: a real-world study. Eur J Nucl Med Mol Imaging 51:2495–2503. https://doi.org/10.1007/s00259-024-06677-y
19. Bakht MK, Beltran H (2025) Biological determinants of PSMA expression, regulation and heterogeneity in prostate cancer. Nat Rev Urol 22:26–45. https://doi.org/10.1038/s41585-024-00900-z
20. Paschalis A, Sheehan B, Riisnaes R, Rodrigues DN, Gurel B, Bertan C, Ferreira A, Lambros MBK, Seed G, Yuan W, Dolling D, Welti JC, Neeb A, Sumanasuriya S, Rescigno P, Bianchini D, Tunariu N, Carreira S, Sharp A, Oyen W, de Bono JS (2019) Prostate-specific membrane antigen heterogeneity and DNA repair defects in prostate cancer. Eur Urol 76:469–478. https://doi.org/10.1016/j.eururo.2019.06.030
21. Afshar-Oromieh A, Babich JW, Kratochwil C, Giesel FL, Eisenhut M, Kopka K, Haberkorn U (2016) The rise of PSMA ligands for diagnosis and therapy of prostate cancer. J Nucl Med 57:79S–89S. https://doi.org/10.2967/jnumed.115.170720
22. Corpetti M, Müller C, Beltran H, de Bono J, Theurillat J-P (2024) Prostate-specific membrane antigen–targeted therapies for prostate cancer: towards improving therapeutic outcomes. Eur Urol 85:193–204. https://doi.org/10.1016/j.eururo.2023.11.018
23. Current K, Meyer C, Magyar CE, Mona CE, Almajano J, Slavik R, Stuparu AD, Cheng C, Dawson DW, Radu CG, Czernin J, Lueckerath K (2020) Investigating PSMA-targeted radioligand therapy efficacy as a function of cellular PSMA levels and intratumoral PSMA heterogeneity, clin. Cancer Res 26:2946–2955. https://doi.org/10.1158/1078-0432.Ccr-19-1485
24. Stuparu AD, Capri JR, Meyer CAL, Le TM, Evans-Axelsson SL, Current K, Lennox M, Mona CE, Fendler WP, Calais J, Eiber M, Dahlbom M, Czernin J, Radu CG, Lückerath K, Slavik R (2021) Mechanisms of resistance to prostate-specific membrane antigen–targeted radioligand therapy in a mouse model of prostate cancer. J Nucl Med 62:989–995. https://doi.org/10.2967/jnumed.120.256263
25. Kratochwil C, Giesel FL, Heussel C-P, Kazdal D, Endris V, Nientiedt C, Bruchertseifer F, Kippenberger M, Rathke H, Leichsenring J, Hohenfellner M, Morgenstern A, Haberkorn U, Duensing S, Stenzinger A (2020) Patients resistant against PSMA-targeting α-radiation therapy often harbor mutations in DNA damage-repair–associated genes. J Nucl Med 61:683–688. https://doi.org/10.2967/jnumed.119.234559
26. Mateo J, Boysen G, Barbieri CE, Bryant HE, Castro E, Nelson PS, Olmos D, Pritchard CC, Rubin MA, de Bono JS (2017) DNA repair in prostate cancer: biology and clinical implications. Eur Urol 71:417–425. https://doi.org/10.1016/j.eururo.2016.08.037
27. Sgouros G, Bodei L, McDevitt MR, Nedrow JR (2020) Radiopharmaceutical therapy in cancer: clinical advances and challenges. Nat Rev Drug Discov 19:589–608. https://doi.org/10.1038/s41573-020-0073-9
28. Durant ST, Zheng L, Wang Y, Chen K, Zhang L, Zhang T, Yang Z, Riches L, Trinidad AG, Fok JHL, Hunt T, Pike KG, Wilson J, Smith A, Colclough N, Reddy VP, Sykes A, Janefeldt A, Johnström P, Varnäs K, Takano A, Ling S, Orme J, Stott J, Roberts C, Barrett I, Jones G, Roudier M, Pierce A, Allen J, Kahn J, Sule A, Karlin J, Cronin A, Chapman M, Valerie K, Illingworth R, Pass M (2018) The brain-penetrant clinical ATM inhibitor AZD1390 radiosensitizes and improves survival of preclinical brain tumor models. Sci Adv 4:eaat1719. https://doi.org/10.1126/sciadv.aat1719
29. Chen G, Zheng D, Zhou Y, Du S, Zeng Z (2024) Olaparib enhances radiation-induced systemic anti-tumor effects via activating STING-chemokine signaling in hepatocellular carcinoma. Cancer Lett 582:216507. https://doi.org/10.1016/j.canlet.2023.216507
30. Huang R-X, Zhou P-K (2020) DNA damage response signaling pathways and targets for radiotherapy sensitization in cancer. Signal Transduct Target Ther 5:60. https://doi.org/10.1038/s41392-020-0150-x
31. Ji J, Ding K, Cheng B, Zhang X, Luo T, Huang B, Yu H, Chen Y, Xu X, Lin H, Zhou J, Wang T, Jin M, Liu A, Yan D, Liu F, Wang C, Chen J, Yan F, Wang L, Zhang J, Yan S, Wang J, Li X, Chen G (2024) Radiotherapy-induced astrocyte senescence promotes an immunosuppressive microenvironment in glioblastoma to facilitate tumor regrowth. Adv Sci (Weinh) 11:2304609. https://doi.org/10.1002/advs.202304609
32. Jayaraman P, Parikh F, Newton JM, Hanoteau A, Rivas C, Krupar R, Rajapakshe K, Pathak R, Kanthaswamy K, MacLaren C, Huang S, Coarfa C, Spanos C, Edwards DP, Parihar R, Sikora AG (2018) TGF-β1 programmed myeloid-derived suppressor cells (MDSC) acquire immune-stimulating and tumor killing activity capable of rejecting established tumors in combination with radiotherapy. Oncoimmunology 7:e1490853. https://doi.org/10.1080/2162402X.2018.1490853
33. Kloosterman DJ, Akkari L (2023) Macrophages at the interface of the co-evolving cancer ecosystem. Cell 186:1627–1651. https://doi.org/10.1016/j.cell.2023.02.020
34. Dias MP, Moser SC, Ganesan S, Jonkers J (2021) Understanding and overcoming resistance to PARP inhibitors in cancer therapy. Nat Rev Clin Oncol 18:773–791. https://doi.org/10.1038/s41571-021-00532-x
35. Jin MH, Oh D-Y (2019) ATM in DNA repair in cancer. Pharmacol Ther 203:107391. https://doi.org/10.1016/j.pharmthera.2019.07.002
36. Beer TM, Kwon ED, Drake CG, Fizazi K, Logothetis C, Gravis G, Ganju V, Polikoff J, Saad F, Humanski P, Piulats JM, Gonzalez Mella P, Ng SS, Jaeger D, Parnis FX, Franke FA, Puente J, Carvajal R, Sengeløv L, McHenry MB, Varma A, van den Eertwegh AJ, Gerritsen W (2016) Randomized, double-blind, phase III trial of ipilimumab versus placebo in asymptomatic or minimally symptomatic patients with metastatic chemotherapy-naive castration-resistant prostate cancer. J Clin Oncol 35:40–47. https://doi.org/10.1200/JCO.2016.69.1584
37. Potluri HK, Ferreira CA, Grudzinski J, Massey C, Aluicio-Sarduy E, Engle JW, Kwon O, Marsh IR, Bednarz BP, Hernandez R, Weichert JP, McNeel DG (2022) Antitumor efficacy of (90) Y-NM600 targeted radionuclide therapy and PD-1 Blockade is limited by regulatory T cells in murine prostate tumors. J Immunother Cancer 10:e005060. https://doi.org/10.1136/jitc-2022-005060
38. Rudqvist N-P, Pilones KA, Lhuillier C, Wennerberg E, Sidhom J-W, Emerson RO, Robins HS, Schneck J, Formenti SC (2018) Demaria, radiotherapy and CTLA-4 Blockade shape the TCR repertoire of tumor-infiltrating T cells. Cancer Immunol Res 6:139–150. https://doi.org/10.1158/2326-6066.CIR-17-0134
39. Franken A, Bila M, Mechels A, Kint S, Van Dessel J, Pomella V, Vanuytven S, Philips G, Bricard O, Xiong J, Boeckx B, Hatse S, Van Brussel T, Schepers R, Van Aerde C, Geurs S, Vandecaveye V, Hauben E, Vander Poorten V, Verbandt S, Vandereyken K, Qian J, Tejpar S, Voet T, Clement PM (2024) Lambrechts, CD4 + T cell activation distinguishes response to anti-PD-L1 + anti-CTLA4

therapy from anti-PD-L1 monotherapy. Immunity 57:541–558e547. https://doi.org/10.1016/j.immuni.2024.02.007
40. Marangoni F, Zhakyp A, Corsini M, Geels SN, Carrizosa E, Thelen M, Mani V, Prüßmann JN, Warner RD, Ozga AJ, Di Pilato M, Othy S, Mempel TR (2021) Expansion of tumor-associated Treg cells upon disruption of a CTLA-4-dependent feedback loop. Cell 184:3998–4015e3919. https://doi.org/10.1016/j.cell.2021.05.027
41. Natale F, Rapp A, Yu W, Maiser A, Harz H, Scholl A, Grulich S, Anton T, Hörl D, Chen W, Durante M, Taucher-Scholz G, Leonhardt H, Cardoso MC (2017) Identification of the elementary structural units of the DNA damage response. Nat Commun 8:15760. https://doi.org/10.1038/ncomms15760
42. Yang K, Halima A, Chan TA (2023) Antigen presentation in cancer — mechanisms and clinical implications for immunotherapy. Nat Rev Clin Oncol 20:604–623. https://doi.org/10.1038/s41571-023-00789-4
43. Borst J, Ahrends T, Bąbała N, Melief CJM, Kastenmüller W (2018) CD4+T cell help in cancer immunology and immunotherapy. Nat Rev Immunol 18:635–647. https://doi.org/10.1038/s41577-018-0044-0
44. Rauch H, Kitzberger C, Janghu K, Hawarihewa P, Nguyen NT, Min Y, Ballke S, Steiger K, Weber WA, Kossatz S (2024) Combining [177Lu]Lu-DOTA-TOC PRRT with PARP inhibitors to enhance treatment efficacy in small cell lung cancer. Eur J Nucl Med Mol Imaging 51:4099–4110. https://doi.org/10.1007/s00259-024-06844-1
45. Hallqvist A, Brynjarsdóttir E, Krantz T, Sjögren M, Svensson J, Bernhardt P (2025) 177Lu-DOTATATE in Combination with PARP Inhibitor Olaparib Is Feasible in Patients with Somatostatin-Positive Tumors: Results from the LuPARP Phase I Trial. J Nucl Med. https://doi.org/10.2967/jnumed.124.268902
46. Sandhu S, Joshua AM, Emmett L, Crumbaker M, Bressel M, Huynh R, Banks PD, Wallace R, Hamid A, Inderjeeth AJ, Tran B, Azad A, Alipour R, Kong G, Ravi Kumar A, Saghebi J, Williams S, Akhurst TJ, Hicks RJ, Hofman MS (2023) LuPARP: phase 1 trial of 177Lu-PSMA-617 and Olaparib in patients with metastatic castration resistant prostate cancer (mCRPC). J Clin Oncol 41:5005–5005. https://doi.org/10.1200/JCO.2023.41.16_suppl.5005